Editors' Suggestion | Featured in Physics

Measuring Entanglement in Physical Networks

Cory Glover[1] and Albert-László Barabási[1,2,3]

[1]Network Science Institute, Northeastern University, Boston, Massachusetts 02115, USA
[2]Department of Network and Data Science, Central European University, Budapest 1051, Hungary
[3]Department of Medicine, Brigham and Women's Hospital, Harvard Medical School, Boston, Massachusetts 02115, USA

(Received 8 March 2024; accepted 27 June 2024; published 13 August 2024)

The links of a physical network cannot cross, which often forces the network layout into nonoptimal entangled states. Here we define a network fabric as a two-dimensional projection of a network and propose the average crossing number as a measure of network entanglement. We analytically derive the dependence of the average crossing number on network density, average link length, degree heterogeneity, and community structure and show that the predictions accurately estimate the entanglement of both network models and of real physical networks.

DOI: 10.1103/PhysRevLett.133.077401

Many complex networks, from the brain [1] to the network of atoms or molecules in materials have true physical manifestation, hence their nodes and links cannot cross each other. While network science offers a series of tools to explore abstract networks like social networks or the World Wide Web, whose links are virtual and whose structure is fully encoded by the adjacency matrix A_{ij}, lately there is a growing interest in understanding physical networks, whose layout and properties are affected by the material nature of their nodes and links [2]. Indeed, volume exclusion and noncrossing conditions [3–5] can force such networks into nonoptimal spatial layouts which they cannot escape, thereby creating entangled networks.

Network entanglement refers to the interdependent relationship between the links of a physical network, where changes in the layout of part of the network affects the positions of the other links. In highly entangled networks the links frequently interfere with one another, leading to knotted structures and nonoptimal layouts. In contrast, in networks with low entanglement the links minimally interfere with one another. Entanglement affects the physical properties of networks, like reducing the network's elastic energy [5], and polymer entanglement can be directly linked with toughness and viscosity [6,7]. More recently, network entanglement has been shown to induce transitions in supercooled water [8]. Understanding the mechanisms influencing entanglement will allow us to design physical networks with predefined entanglement, modulating certain physical properties, as well as help us better understand the physical properties of real physical networks.

Here we investigate how the network embedding, defined by the detailed spatial layout of its nodes and links, and the network topology, captured by A_{ij}, affect network entanglement. We begin by defining a *network fabric* as a two-dimensional projection of a physical network. As a physical network can have infinitely many fabrics, depending on the projection angle, inspired by knot theory [9,10], we propose the average crossing number (ACN) [11,12] as a measure of its degree of entanglement. We derive analytically the dependence of entanglement on the network's density, link length, degree heterogeneity, and community structure. Finally, we show that the developed analytical framework can predict changes in entanglement of both network models and real physical networks.

Previous work estimated network entanglement using the graph linking number (GLN) [5], which has an exponentially growing complexity $O(e^N)$ [13] and is not easily amenable to mathematical treatment. Here we show that fabrics allow us to introduce a new entanglement metric, the average crossing number (ACN), which is significantly faster, having complexity $O(L^2)$. A network fabric f is any two-dimensional projection of a physical network such that each crossing point maintains the over and under crossing information [Fig. 1(a) and [13]]. The

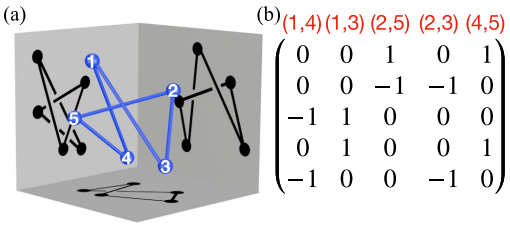

FIG. 1. (a) Three possible fabrics of a simple five cycle. Each projection to a different plane results in a different fabric with different crossings. (b) The crossing matrix of the fabric in the left projection. Each row and column corresponds to a link in the physical network. To calculate the average crossing number, we average the number of crossings in each fabric. For the three fabrics shown in the figure, the five cycle has $\langle m \rangle \approx 2.66$.

average crossing number (ACN) of a network is $\langle m\rangle = (1/4\pi r^2)\int_{S^2} m(f)dS$ [11], where $m(f)$ is the number of crossings in the fabric f, dS is the area form of the sphere S^2 and r is the radius of the sphere that holds the network. In other words, $\langle m\rangle$ is the average number of link intersections over all possible fabrics (projections).

To estimate $\langle m\rangle$ for a given physical network, we take a projection and count the crossings in the resulting fabric using the crossing matrix, $R \in \mathbb{R}^{L\times L}$, whose entries are 1 if the row link crosses over the column link, -1 if the row link crosses under the column link, and 0 if the two links do not intersect [Fig. 1(b)]. We then average $m(f)$ over multiple fabrics to estimate the average crossing number. We find that the ACN is self-averaging for large system sizes [13] and it correlates with the linking among loops [13], suggesting that the crossings in a fabric directly informs our understanding of network entanglement.

For simplicity and without loss of generality, we focus on linear physical networks (LPNs), whose links are straight lines, and assume that each link has infinitesimally small thickness. This allows us to focus on the effects of the network layout and topology on entanglement while avoiding the effects of volume. Note that any nonlinear physical network can be approximated with a LPN by adding ghost nodes along curved links, hence our results can be generalized to networks with curved links.

The network layout affects the probability that two links can cross, which we can analytically calculate for random layouts [13] using Sylvester's four point problem [25]. However, real networks are not randomly embedded but follow an optimal layout, obtained by minimizing the network's total link length, which captures the system's elastic energy [4,26–28].

The longer a link, the higher likelihood that it will cross other links, suggesting that the probability that each link pair will cross must scale with the average link length $\langle l\rangle$ [13]. Because real physical networks have widely different length scales, we normalize $\langle l\rangle$ by the average distance between two nodes $\langle l\rangle^* = \langle l\rangle/\langle d\rangle$. As random layouts with higher $\langle l\rangle$ should have more crossings than optimal layouts with minimal $\langle l\rangle$, for random layouts $\langle l\rangle^* \to 1$ and for optimal layouts $\langle l\rangle^* \ll 1$. We then write $\langle m\rangle \sim \langle l\rangle^* m_{\max}$, where $m_{\max}$ is the maximum number of possible link pairs and $\langle l\rangle^*$ scales with the probability that the pair crosses.

In a LPN, if two links connect to the same node, they cannot cross elsewhere. Hence, $m_{\max} = \binom{L}{2} - \sum_{i\in V(G)}\binom{k_i}{2}$ [29]. Here the first term is the total number of link pairs and the second term removes the pairs which connect to the same node. We expand this bound to [13]

$$m_{\max} = \frac{L(L-1)}{2} - \frac{N}{2}\langle k^2\rangle + \frac{N}{2}\langle k\rangle, \tag{1}$$

where $\langle k\rangle$ and $\langle k^2\rangle$ are the moments of the degree distribution $P(k)$.

Nodes in real networks often form communities, representing subgraphs whose nodes share some common properties or roles [30], and hence tend to be connected to each other. In optimal energy layouts, these communities often separate in space [26]. As links within the same community are more likely to cross each other than they are to cross links in different communities, this suggests that the presence of communities reduces $m_{\max}$. To capture this reduction, consider a network with C equal-sized communities where each link in the network connects two nodes in distinct communities with probability p. Then $(1-p)L$ links only cross links within their own community while pL links can cross any link, reducing $m_{\max}$ to [13]

$$m_{\max} \approx \frac{(1-p)^2L^2}{2C} + 2pL^2 - \sum_i \binom{k_i}{2}. \tag{2}$$

Combining (1) and (2), we arrive at our key result, approximating the impact of the network layout and topology on LPN entanglement. Defining $\langle m\rangle^* = \langle m\rangle/L^2$ as the normalized ACN, we obtain

$$\langle m\rangle^* \sim \langle l\rangle^*\left(\frac{(1-p)^2}{C} + 2p - \frac{\langle k^2\rangle}{N\langle k\rangle^2} + \frac{1}{N\langle k\rangle}\right). \tag{3}$$

This result highlights the combined impact of the network's embedding and topology on the network's entanglement. Furthermore, it helps us understand the variables which control entanglement. Indeed, networks where $\langle m\rangle^* \to 0$ leads to less entangled and more optimal layouts. In contrast, networks with $\langle m\rangle^* \to 1$ correspond to highly entangled structures. To test the validity of (3), we examine separately the role of the average link length, degree heterogeneity, and community structure.

Average link length—Networks with the same adjacency matrix A_{ij} can have layouts with different $\langle l\rangle^*$. To test the effect of $\langle l\rangle^*$ on the ACN, we generate different embeddings of the same network, each with a specified average link length $\langle l\rangle^*$, using simulated annealing [13]. We measure the normalized ACN $\langle m\rangle^*$ for each embedding. As shown in Fig. 2(a), we find a linear relationship between $\langle l\rangle^*$ and $\langle m\rangle^*$ for both ER, BA, and configuration model networks, evidence that Eq. (3) correctly captures the ACN's dependence on $\langle l\rangle^*$ for networks with different layouts.

Degree heterogeneity—A remarkable feature of Eq. (3) is its dependence on $\langle k^2\rangle$, indicating the unexpected role of degree heterogeneity and hubs in entanglement. Indeed, while network robustness [31,32] and epidemic spreading [33] are known to depend on $\langle k^2\rangle$, in physical networks the role of degree heterogeneity remains unknown. Indeed, heterogeneity's role on LPNs emerges because links connected to a hub cannot cross. Hence, hubs reduce the number of possible crossings. In the extreme case of a star

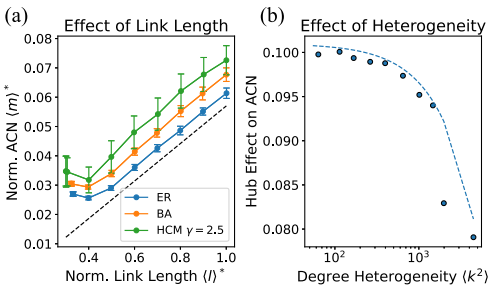

FIG. 2. (a) The average link length for networks, generated by the ER, BA, and configuration models with $N = 10^3$ and $\langle k \rangle = 6$, embedded using simulated annealing and compared with the normalized ACN. The black dashed line corresponds to a linear fit $y = 0.06x - 0.01$. (b) We generate networks with $N = 10^5$ and $P(k) \sim k^{-\gamma}$ using a hypercanonical configuration model with $\gamma = 2.01$. The plot shows $\langle k^2 \rangle$ versus $(\langle m \rangle^*/\langle l \rangle^*)$ and the dotted line is the analytical prediction (3).

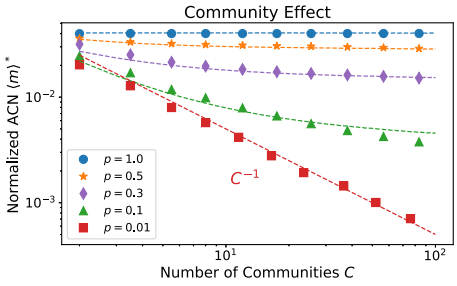

FIG. 3. The normalized ACN for networks ($N = 5000$) with varying degree of intercommunity connections (p). The dashed line corresponds to the prediction of curve Eq. (3).

network, where all nodes are connected to a single hub, no links can cross and the ACN is zero.

Equation (3) predicts the effect of heterogeneity for different network models. Assume each model exhibits no community structure. In regular or random regular networks ($k_i = k$) [34], we have $\langle k^2 \rangle = \langle k \rangle^2$, hence as $N \to \infty$, $\langle m \rangle \sim (N\langle k \rangle)^2 \langle l \rangle^*$. In ER random networks [35], where each link exists with probability p, $\langle k \rangle = \langle k \rangle (1 + \langle k \rangle)$, thus, the leading term becomes $N(N-1)\langle k \rangle^2 \langle l \rangle^*$. In a scale-free network where the degree sequence is a power law with degree exponent γ [36], we have $\langle k^2 \rangle \sim N^{[1/(\gamma-1)]}$; hence, ACN scales as $(N\langle k \rangle)^2 \langle l \rangle^* \left[1 - N^{[(4-2\gamma)/(\gamma-1)]} + 1/(N\langle k \rangle)\right]$. When $\gamma < 3$ the second moment diverges with the network size, resulting in a potentially significant reduction of the ACN.

To verify the role of degree heterogeneity, we generate networks with $N = 10^5$ using a hypercanonical configuration model, which generates a network with a predefined degree sequence drawn from a power-law degree distribution [37]. For each network we measure $\langle m \rangle^*/\langle l \rangle^*$, finding that the dependence of $\langle m \rangle^*$ on $\langle k^2 \rangle$ is well captured by Eq. (3) [see Fig. 2(b)].

Community structure—Optimal network embeddings with community structure reduce entanglement by forcing links into distinct communities. To test the role of community structure on the ACN, we generate networks with C isolated, homogeneous communities. Each link is then rewired to a random node in the network with probability p, representing an intercommunity link. As shown in Fig. 3, we find that when $p \to 0$, $\langle m \rangle \sim C^{-1}$ as predicted in Eq. (3). For $p \to 1$, C has no effect. For intermediate p values, we find that $\langle m \rangle \sim (1-p)^2 C^{-1} + 2p$ offers an excellent approximation, as predicted by Eq. (3) [13].

Taken together, we find that both degree heterogeneity and communities reduce network entanglement. To test the accuracy of Eq. (3) as a whole, we generated networks using a variety of network models exhibiting varying levels of degree heterogeneity and community structure. For each network, we predict the ACN using (3) and calculate the true ACN numerically. We embed each network with an optimal noncrossing layout offered by an accelerated force-directed layout [26] and FUEL algorithm [4] as well as in a random layout. We estimate C with the number of connected components. Each network's ACN is then predicted for $p = 0$ and $p = 1$, obtaining a range of possible estimated ACN values. For each network model, the prediction (3) is close to the true ACN for both optimal and random layouts (Fig. 4).

Finally, we repeat the above procedure for real physical networks [13] and for the flavor network, a network with high heterogeneity and strong community structure, using a previously published optimal layout [26]. In general, we have a range of methods to identify communities [30,38,39]. Here, we estimate the number of communities C by maximizing the modularity of the network. Again, we find a good agreement between the predicted and true ACN (Fig. 4), results that hold for the normalized ACN as well [13].

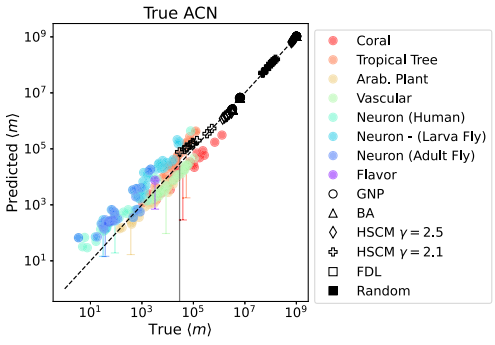

FIG. 4. The predicted ACN by Eq. (3) (vertical axis) for various real datasets, the flavor network, a BA network, an ER network, and two hypercanonical configuration models versus the empirically measured ACN (horizontal axis). Each synthetic network has 1000 nodes with average degree $\langle k \rangle = 6$. The black dashed line is the diagonal. For each dataset we compute the ACN for $p = 0$ and $p = 1$, represented by the error bar (one for each dataset). For datasets, the data point is for $p = 1$.

We find that the ACN is strongly correlated with the graph linking number (GLN), an earlier measure of network entanglement, making it a suitable alternative. The GLN suffers from high computational complexity, $O(e^N)$. In contrast, the complexity of the ACN if $O\big((L^2 - N\langle k^2\rangle + N\langle k\rangle)f\big)$, where f is the number of fabrics averaged over. For example, in a sparse network with $N \sim L = 20$, computing the GLN takes approximately the same time as computing the ACN on a network with 20 000 nodes. Finally, GLN $= 0$ for loopless networks, while the ACN captures the entanglement of networks without loops as well and can be analytically estimated via Eq. (3) [13].

Also note that degree heterogeneity reduces the computational complexity of the ACN. To test this prediction, we generated networks with degree distribution drawn from a power law with varying degree exponent γ, finding that small γ has lower computational cost [13].

In conclusion, we have shown how the entanglement of a physical network is simultaneously affected by the network layout and the network topology. While network density $(N\langle k\rangle)^2$ sets the magnitude of entanglement, hubs and community structure reduce its value.

We also want to emphasize some limitations and avenues for improvement. Because of the simplifying assumptions of $\langle m\rangle$ [13], the predictions in Fig. 4 are designed to unveil the scaling of the ACN rather than exact value of the ACN. Furthermore, for neurons, tropical trees, and the flavor network, the community structure must be accounted for to obtain a more accurate estimate.

Therefore, our results can be further improved by examining how to measure the community structure and estimate p using both the network layout and topology, further enhancing the predictive power of Eq. (3). Presently Eq. (3) only offers a bounded range on the possible ACN. Also, we assumed that $\langle l\rangle^*$, degree heterogeneity, and community structure are independent variables, which is not generally true [13,40]. Furthermore, understanding the impact of degree heterogeneity and community structure on $\langle l\rangle^*$ will glean better insight into the full role of network topology on the ACN. Additionally, these results should be further examined using a larger variety of realistic network models, including hyperbolic networks [41,42], where both degree heterogeneity, community structure, and clustering can be simultaneously controlled, as well as other real systems with greater degree heterogeneity [13]. Finally, there is need to further investigate the role entanglement has on physicality in order to inform network designs in novel material systems.

Acknowledgments—We thank Jinha Park for his initial exploration of fabric projections to study nonisotopic layouts of networks. We also thank Márton Pósfai, Ivan Bonamassa, Csaba Both, and Harrison Hartle for helpful discussions regarding this work. This research was supported by the NSF Grant No. 2243104—COMPASS. A. L. B. is also supported by the European Union's Horizon 2020 research and innovation program No. 810115—DYNASNET.

[1] E. K. Towlson, P. E. Vértes, S. E. Ahnert, W. R. Schafer, and E. T. Bullmore, JNeurosci **33**, 6380 (2013).
[2] D. L. Barabási, G. Bianconi, E. Bullmore, M. Burgess, S. Chung, T. Eliassi-Rad, D. George, I. A. Kovács, H. Makse, T. E. Nichols *et al.*, JNeurosci **43**, 5989 (2023).
[3] M. Pósfai, B. Szegedy, I. Bačić, L. Blagojević, M. Abért, J. Kertész, L. Lovász, and A.-L. Barabási, Nat. Phys. **20**, 142 (2024).
[4] N. Dehmamy, S. Milanlouei, and A.-L. Barabási, Nature (London) **563**, 676 (2018).
[5] Y. Liu, N. Dehmamy, and A.-L. Barabási, Nat. Phys. **17**, 216 (2021).
[6] D.-C. Kong, M.-H. Yang, X.-S. Zhang, Z.-C. Du, Q. Fu, X.-Q. Gao, and J.-W. Gong, Macromol. Mater. Eng. **306**, 2100536 (2021).
[7] D. Grijpma, J. Penning, and A. Pennings, Colloid Polym. Sci. **272**, 1068 (1994).
[8] A. Neophytou, D. Chakrabarti, and F. Sciortino, Nat. Phys. **18**, 1248 (2022).
[9] C. C. Adams, *The Knot Book* (American Mathematical Society, Providence, 1994).
[10] T. Fleming and B. Mellor, Intrinsic linking and knotting in virtual spatial graphs, *Algebraic & Geometric Topology* (2007).
[11] G. Buck and J. Simon, Topol. Appl. **91**, 245 (1999).
[12] J. O'hara, *Energy of Knots and Conformal Geometry* (World Scientific, Singapore, 2003), Vol. 33.
[13] See Supplemental Materials at http://link.aps.org/supplemental/10.1103/PhysRevLett.133.077401, which includes Refs. [14–24], for (i) analysis of the relationship between the graph linking number and the ACN, (ii) evidence of self-averaging in the ACN, (iii) detailed analytical derivation of Eq. (3), (iv) explanation of simulated annealing pipeline, (v) analysis of the relationship between degree heterogeneity and average link length, (vi) analytical derivation of scaling of the ACN, (vii) details of physical network data analyzed, (viii) further experiments measuring the normalized ACN, and (ix) exploration of the ACN using hyperbolic models.
[14] G. Bianconi and M. Marsili, J. Stat. Mech. (2005) P06005.
[15] M. Schaefer, Electron. J. Comb. DS21 (2012).
[16] S. Watson, Mathematical Questions and their Solutions from the Educational Times **4**, 101 (1865).
[17] W. Woolhouse, Mathematical Questions and their Solutions from the Educational Times **7**, 81 (1867).
[18] E. Ravasz and A.-L. Barabási, Phys. Rev. E **67**, 026112 (2003).
[19] F. D. Malliaros and M. Vazirgiannis, Phys. Rep. **533**, 95 (2013).
[20] L. Peel, D. B. Larremore, and A. Clauset, Sci. Adv. **3**, e1602548 (2017).
[21] G. Palla, I. Derényi, I. Farkas, and T. Vicsek, Nature (London) **435**, 814 (2005).

[22] H. Seyed-Allaei, G. Bianconi, and M. Marsili, Phys. Rev. E **73**, 046113 (2006).
[23] H. Pan, F. Hétroy-Wheeler, J. Charlaix, and D. Colliaux, Arabidopsis 3d + t dataset, 10.5281/zenodo.5205561 (2021).
[24] J. Gonzalez de Tanago, A. Lau, H. Bartholomeus, M. Herold, V. Avitabile, P. Raumonen, C. Martius, R. C. Goodman, M. Disney, S. Manuri *et al.*, Methods Ecol. Evol. **9**, 223 (2018).
[25] R. E. Pfiefer, Math. Mag. **62**, 309 (1989).
[26] C. Both, N. Dehmamy, R. Yu, and A.-L. Barabási, Nat. Commun. **14**, 1560 (2023).
[27] W. T. Tutte, Proc. London Math. Soc. **3**, 743 (1963).
[28] S. Horvát, R. Gămănuţ, M. Ercsey-Ravasz, L. Magrou, B. Gămănuţ, D. C. Van Essen, A. Burkhalter, K. Knoblauch, Z. Toroczkai, and H. Kennedy, PLoS Biol. **14**, e1002512 (2016).
[29] S. R. Peddada, N. M. Dunfield, L. E. Zeidner, K. A. James, and J. T. Allison, in *International Design Engineering Technical Conferences and Computers and Information in Engineering Conference* (American Society of Mechanical Engineers, New York, 2021), Vol. 85383, p. V03AT03A042.
[30] S. Fortunato, Phys. Rep. **486**, 75 (2010).
[31] R. Cohen, K. Erez, D. Ben-Avraham, and S. Havlin, Phys. Rev. Lett. **85**, 4626 (2000).
[32] G. Caldarelli, *Scale-Free Networks: Complex Webs in Nature and Technology* (Oxford Finance, Oxford, 2007).
[33] M. Boguná, R. Pastor-Satorras, and A. Vespignani, Phys. Rev. Lett. **90**, 028701 (2003).
[34] J. H. Kim and V. H. Vu, in *Proceedings of the Thirty-Fifth ACM Symposium on Theory of Computing* (ACM Press, New York, 2003), pp. 213–222.
[35] E. N. Gilbert, Ann. Math. Stat. **30**, 1141 (1959).
[36] R. Albert and A.-L. Barabási, Rev. Mod. Phys. **74**, 47 (2002).
[37] I. Voitalov, P. Van der Hoorn, M. Kitsak, F. Papadopoulos, and D. Krioukov, Phys. Rev. Res. **2**, 043157 (2020).
[38] P. Villegas, T. Gili, G. Caldarelli, and A. Gabrielli, Nat. Phys. **19**, 445 (2023).
[39] R. Burioni and D. Cassi, J. Phys. A **38**, R45 (2005).
[40] A.-L. Barabási, Z. Dezső, E. Ravasz, S.-H. Yook, and Z. Oltvai, in *AIP Conference Proceedings* (AIP Publishing, Melville, 2003), Vol. 661, pp. 1–16.
[41] F. Papadopoulos, M. Kitsak, M. Á. Serrano, M. Boguná, and D. Krioukov, Nature (London) **489**, 537 (2012).
[42] D. Krioukov, F. Papadopoulos, M. Kitsak, A. Vahdat, and M. Boguná, Phys. Rev. E **82**, 036106 (2010).